ACADEMIC PRESS

Available online at www.sciencedirect.com
SCIENCE DIRECT®

Journal of Catalysis 218 (2003) 209–219

JOURNAL OF CATALYSIS

www.elsevier.com/locate/jcat

X-ray absorption and NMR spectroscopic investigations of zinc glutarates prepared from various zinc sources and their catalytic activities in the copolymerization of carbon dioxide and propylene oxide

Jong-Seong Kim,[a] Moonhor Ree,[a,*] Tae Joo Shin,[a] Oc Hee Han,[b] Sung June Cho,[c,1] Yong-Taek Hwang,[a] Joong Yeon Bae,[a] Jae Min Lee,[a] Ryong Ryoo,[c] and Heesoo Kim[d]

[a] *Department of Chemistry, School of Environmental Science & Engineering, Center for Integrated Molecular Systems, Polymer Research Institute, BK21 Program, Division of Molecular and Life Science, and Pohang Accelerator Laboratory, Pohang University of Science and Technology, San 31, Hyoja-dong, Pohang 790-784, Republic of Korea*

[b] *Korea Basic Science Institute, 52 Yeoeun-dong, Yusung-gu, Daejeon 305-333, Republic of Korea*

[c] *Department of Chemistry, Korea Advanced Institute of Science & Technology, 373-1 Kusung-dong, Yusung-gu, Daejeon 305-701, Republic of Korea*

[d] *Department of Microbiology, Dongguk University College of Medicine, 707 Seokjang-dong, Kyeongju 780-714, Republic of Korea*

Received 25 November 2002; revised 20 February 2003; accepted 24 February 2003

Abstract

The local and microstructures of zinc glutarates synthesized from various zinc sources were investigated by X-ray absorption and solid-state carbon-13 nuclear magnetic resonance spectroscopy, and related to their catalytic activities in the copolymerization of carbon dioxide and propylene oxide. It was found that the local structure around the Zn atoms of the zinc glutarate catalysts consists basically of tetrahedrally coordinated carboxyl oxygen atoms with a Zn–O bond distance in the range 1.95–1.96 Å, and that the nearest neighbor Zn atom distance is 3.19–3.23 Å. These results suggest that the catalysts have a network structure composed of layers interconnected by glutarate ligands. However, the first-shell structures of the catalysts tested are somewhat different, which might originate from differences in the catalysts' overall crystallinity and crystal quality (crystal size and perfection) produced by their different synthetic routes. The surface areas of the catalysts also varied with synthetic route. In the copolymerization, one catalyst with low surface area but the highest crystallinity and best crystal quality shows the highest catalytic activity, which is contrary to the usual expectation of increased catalytic activity with increased catalyst surface area. Therefore, the catalytic activities of zinc glutarates in the copolymerization seem to depend primarily on their morphological structures rather than on their surface areas. The surface areas of zinc glutarates may play a crucial role in improving the catalytic activity in the copolymerization when they first meet the morphological requirements (i.e., high crystallinity and crystal quality).

Keywords: Zinc glutarate catalyst; XANES; EXAFS; Solid-state CP MAS ^{13}C NMR; Copolymerization of CO_2 with propylene oxide

1. Introduction

Human activities add about 24 billion tons of CO_2 annually to the atmosphere, with 22 billion tons produced annually by the burning of fossil fuels [1]. These CO_2 emissions are believed to cause the greenhouse effect, which contributes greatly to climate change [2–6]. Hence, CO_2 is regarded as an environmental pollutant, and the immediate reduction of CO_2 emissions has been seriously considered by all nations of the world [1,3,6–9]. On the other hand, techniques for the capture and disposal of CO_2 are actively sought as a means to avoid releasing this greenhouse gas into the atmosphere [8,10]. However, from the standpoints of economy and ecology, the utilization of CO_2 is more desirable than its disposal.

One possible approach to utilization is the production of polymeric materials from CO_2 resources and the use of these polymer products in daily life and industry. Of course, the amount of CO_2 fixation into polymer products will only ever be small in comparison to the amount produced by burning fossil fuels, but may nevertheless be useful, depending

* Corresponding author.
E-mail address: ree@postech.edu (M. Ree).
[1] Present address: Department of Applied Chemistry Chonnam National University, Gwangju 500-757, Republic of Korea.

0021-9517/03/$ – see front matter
doi:10.1016/S0021-9517(03)00082-4

on the usage of the polymer products. The copolymerization of CO_2 with oxiranes is one method by which CO_2 can be chemically fixed into polymeric materials [11–33]. The copolymerization of CO_2 with an oxirane, propylene oxide (PO), was first described in 1969 by Inoue and co-workers, who used Et_2Zn/H_2O as a catalyst [11]. CO_2 is relatively stable, so copolymerization of CO_2 with oxiranes requires a very active catalyst. This situation has prompted efforts to find a highly active catalyst suitable for such copolymerizations. A variety of candidate organometallic catalysts and their precursors have been reported [12–36]. Among the catalysts reported to date, zinc glutarate has been found to be the most effective, economically feasible catalyst for the production of aliphatic polycarbonates with reasonably high molecular weights [13,14,18,19,24,35,36]. We have recently reported a highly efficient process for synthesizing polycarbonate from CO_2 using PO as a comonomer and reaction medium with zinc glutarate as a catalyst [30,32]. This synthetic process gave a very high yield, 70 g of polymer per gram of catalyst. For this process the polymer yield was increased double by using a zinc glutarate catalyst in a size of 0.2–0.3 μm; the catalyst was prepared from zinc oxide and glutaric acid and then fragmented by ball-milling or ultrasonication [35].

However, zinc glutarate catalysts are generally insoluble in solvents other than highly acidic solutions (pH < 2). In highly acidic solutions, the catalyst dissolves via dissociation; thus, zinc glutarate acts as a heterogeneous rather than homogeneous catalyst in the polymerizations. In general, the performance of heterogeneous catalysts is influenced by their morphological structures and the chemical nature of the reaction system. The term "morphological structure" refers principally to crystalline dimension as well as to surface area. It has previously been reported that zinc glutarates of lower surface area but higher crystallinity produce more polymerization activity than catalysts with the opposite properties [30]. Therefore, for zinc glutarates, crystalline structure may function as the crucial factor determining the activity of the catalyst. However, the detailed crystal structures of these catalysts that are critical to understanding their catalytic activity have not yet been determined, because these catalysts are always obtained as powders rather than as single crystals. The determination of the structures of the zinc glutarates carried out in the present work is vital to the understanding of their high catalytic activities in the copolymerization of CO_2 with oxiranes.

In this work, we prepared zinc glutarate catalysts from various zinc and glutarate sources through different synthetic methods, and additionally synthesized zinc monomethylglutarate. The structures of the resulting zinc gluterates were then characterized using X-ray absorption near-edge structure (XANES) and extended X-ray absorption fine structure (EXAFS) spectroscopies as well as solid-state ^{13}C nuclear magnetic resonance (NMR) spectroscopy with cross-polarization (CP), magic angle spinning (MAS), and proton decoupling. The synthesized catalysts were tested in the copolymerization of CO_2 and PO in order to determine the relationships between their morphological structures and their catalytic activities.

2. Experimental

2.1. Materials

Carbon dioxide (purity greater than 99.8%) was obtained from both Aldrich Company and BOC Gases Company (Korea), and propylene oxide was obtained from SK Oxichemical Company (Korea). All other chemicals used in this study were purchased from Aldrich. In particular, diethylzinc was received packaged in *Sure/Pac* metal cylinders. PO was purified by distillation over calcium hydride under dry nitrogen gas before use. Toluene, benzene, ethanol, 1,4-dioxane, tetrahydrofuran, and glutaric anhydride were purified by the usual methods before use. All other chemicals were used as received. Zinc oxide and zinc hydroxide were ground into fine powders with a mortar and pestle before use.

2.2. Synthesis of catalysts

Zinc glutarate was synthesized by four different methods as described elsewhere [30,32] (Table 1). In the first method, zinc glutarate (ZnGA-1) was prepared from zinc oxide (ZnO) and glutaric acid (GA). Briefly, 98 mmol of GA (purity greater than 99%) was dissolved in 150 mL of toluene in a round-bottom flask (250 mL) equipped with a Dean-Stark trap and a reflux condenser with a drying tube. Then, 100 mmol of ZnO (purity 99.99%) as a fine powder was added into the GA/toluene solution. After the addition was complete, the slurried mixture was stirred vigorously at 55 °C for 2 h and then heated and refluxed until there were no further drops of water (reaction by-product) in the Dean-

Table 1
Preparation of zinc glutarates from various zinc compounds and glutaric acid derivatives

Cat. No.	Zinc compound (mmol)	Glutaric acid derivative (mmol)	Solvent (ml)	Reaction temperature (°C)	Reaction time (h)	Yield (%)
ZnGA-1	ZnO (100)	Glutaric acid (98)	Toluene (150)	55	4	98
ZnGA-2	$Zn(NO_3)_2 \cdot 6H_2O$ (20)	Glutaric anhydride (120)	THF[a] (140)	67	12	100
ZnGA-3	$ZnEt_2$ (20)	Glutaric acid (20)	Dioxane (140)	25	12	100
ZnGA-4	ZnO (20)	Monomethylglutarate (39)	Benzene (140)	80	24	62

[a] Tetrahydrofuran.

Stark trap. After cooling to room temperature, the reaction mixture was filtered and washed with acetone several times, giving zinc glutarate in powder form. The reaction yield was estimated from the amount of unreacted glutaric acid found after removal of the used toluene and acetone from the filtrate as 100%.

In the second method, 20 mmol of zinc nitrate [$Zn(NO_3)_2 \cdot 6H_2O$; purity > 98%] was dissolved in 20 mL of tetrahydrofuran (THF); this solution was slowly added into 120 mmol of glutaric anhydride (GAn) in 120 mL of THF. The reaction mixture was maintained at 67 °C for 12 h. The nitric acid gas by-product was trapped in a flask filled with water, which was connected to the condenser attached to the reaction flask by a rubber tube. The reaction product was filtered off, followed by washing with THF several times. Zinc glutarate (ZnGA-2) was obtained with a yield of 98%, as calculated from the zinc nitrate loading.

In the third method, zinc glutarate was prepared from $ZnEt_2$ and GA. GA (20 mmol) in 20 mL of 1,4-dioxane was slowly added with vigorous stirring into a solution of $ZnEt_2$ (20 mmol) in 50 mL of 1,4-dioxane that had been cooled to 0 °C using an ice bath. After the addition was completed, the ice bath was removed. The reaction mixture was then stirred continuously for 12 h at room temperature. The product was filtered off, followed by washing several times with 1,4-dioxane. Zinc glutarate (ZnGA-3) was obtained with a yield of 100%, as calculated from the $ZnEt_2$ loading.

In the last method, zinc monomethylglutarate (ZnGA-4) was prepared from ZnO and monomethylglutarate. In this synthesis benzene was used as the solvent instead of toluene. Monomethylglutarate (39.2 mmol) was added to ZnO (20 mmol) suspended in 140 mL of benzene. The reaction temperature and time were 80 °C and 24 h, respectively. The reaction yield was 62%.

The powdered zinc glutarate products were dried in a vacuum of 1×10^{-5} Torr at 100 °C for 2 days. The dried zinc glutarate products were ground up using a mortar and pestle, resulting in fine powders. The size of the particles in the powders was determined by optical microscopy to be 2–3 μm. The finely powdered catalysts were further dried for 3 days at 100 °C in a vacuum of 1×10^{-5} Torr before use.

The synthesized catalysts were characterized by Fourier-transform infrared (FTIR) spectroscopy: FTIR (KBr), 1585 cm^{-1} (COO^- antisymmetric stretching), 1536 cm^{-1} (COO^- antisymmetric stretching), 1405 cm^{-1} (COO^- symmetric stretching), 2957 cm^{-1} (CH stretching), and 1458 cm^{-1} (CH_2 scissoring). Carbonyl (C=O) stretching (1697 cm^{-1}), a vibrational peak characteristic of glutaric acid and glutaric anhydride, was not detected.

2.3. Copolymerization of CO_2 and PO using the synthesized catalysts

The polymerization experiments were carried out in a Parr 500 mL autoclave high-pressure reactor equipped with a magnetic stirring unit. Prior to reaction, both the autoclave and the catalyst were dried at 100 °C for 3 days in a vacuum oven at 1×10^{-5} Torr, followed by charging with dry nitrogen gas just before transfer into the reactor. Then the dried reactor body and the catalyst were quickly transferred into the glovebox (dry) containing the reactor head, followed by further drying for 4 h under vacuum. After drying, the glovebox (dry) was purged with dry nitrogen gas. The dried zinc glutarate catalyst (1.00 g) was added into the reactor, followed by the addition of the desired amount of purified PO using a syringe. Then, the reactor was capped by the reactor head and the entire assembly was transferred to a pressure cell. The reactor was connected to dry nitrogen and CO_2 cylinders using a three-way valve. The reactor was pressurized to 51.5 atm with CO_2 after the connection pipelines were cleaned out with dry nitrogen gas. Then the reactor was heated at 60 °C with stirring. After 40 h, the reactor was cooled to room temperature, and the pressure was released. The unreacted PO was recovered from the reactor into a flask under low vacuum. The polymer product was taken out and dried further in a vacuum oven at room temperature, followed by weighing to determine gross yield. The dried product was dissolved in approximately 400 mL of methylene chloride and transferred to a separating funnel. The catalyst residue was extracted from the product solution by adding approximately 400 mL of dilute hydrochloric acid. The extraction was repeated three times. The product solution was subsequently washed two times with approximately 400 mL of distilled water. The product solution was concentrated to an appropriate volume using a rotary evaporator. Then the product solution was poured into an excess of methanol. The polymer precipitate was filtered off, followed by drying at room temperature in a vacuum oven. The solvents used were removed from the filtrate by distillation, giving a polymer product that was soluble in methanol.

2.4. Measurements

X-ray absorption spectroscopic measurements were carried out at the 3C1 beamline (BL) [37] of the Pohang Light Source (PLS) facility (at Pohang University of Science and Technology, Korea) with ring current in the range 120–170 mA at 2.5 GeV power. X-ray beams from a bending magnet of the PLS storage ring were monochromatized with a Broomstick double-crystal monochromator with detuning to 85% intensity to eliminate higher order harmonics [37]. The typical energy resolution ($\Delta E/E$) was 2×10^{-4} at 10 keV. The incident and transmitted X-ray intensities were measured with the ionization chambers filled with 100% N_2 and a mixed gas (70% N_2 + 30% He), respectively. The photon energy was corrected for E_0, which is the first zero of the second derivative in the X-ray absorption. The catalyst samples were transformed into self-supporting wafers of diameter 10 mm using a mechanical presser, in order to avoid the leakage effect. X-ray absorption spectra were obtained at the Zn K-edge in transmission mode. The X-ray absorption data in the wave vector (k) range 3

to 14 $Å^{-1}$ were analyzed using the UWX AFS2 program package [38]. The extended X-ray absorption fine structure spectrum was multiplied by the weighting scheme (k^3) after background removal and normalization. Background was removed with an r-space technique that minimizes low r background components in the Fourier transform (FT) through comparison with a standard EXAFS spectrum generated using the FEFF5 code [39]. This procedure is described in detail elsewhere [40].

Solid-state ^{13}C NMR spectroscopic experiments were carried out with a Bruker DSX 400 instrument (Bruker Analytische Messtechnik GmbH, Germany) at 9.4 T and room temperature. The proton radiofrequency (RF) field strength for cross-polarization and the decoupling strength were both 50 kHz, resulting in a 5 µs 90° pulse length. Pulse repetition delay, proton flip pulse, and contact time for the cross-polarization magic-angle spinning experiments were 10 s, 5 µs, and 3 ms, respectively. The typical spinning rates employed were 6.5 or 7 kHz. Carbon chemical shifts were referenced to external neat tetramethylsilane (TMS). The full widths at half height (FWHH) of peaks were measured from deconvoluted spectra with a Lorentzian lineshape; the 5 Hz line broadening applied to the free induction decay signal during Fourier transform processing was subtracted to obtain $FWHH_{obj}$. The chemical-shift inhomogeneity of the catalysts was calculated from the $FWHH_{inh}$ obtained by subtracting the FWHH due to the T_2 effect from $FWHH_{obj}$. T_2 was obtained from the arrayed spin–echo delay values that were integer multiples of a rotor period. Relaxation times $T_1(^{13}C)$, $T_{1\rho}(^{13}C)$, and $T_{1\rho}(^{1}H)$ were taken at a spinning rate of 6.5 kHz with CP-MAS pulse sequences as described elsewhere [41]. The spin–lock RF fields for the $T_{1\rho}$ measurements were 50 kHz.

In addition, the surface areas of the catalysts were determined by the Brunauer–Emmet–Teller (BET) technique using a Micrometrics BET analyzer (ASAP 2010), as described elsewhere [42]. Nitrogen gas was used as the absorbed molecule.

For the polymer products we obtained, number average molecular weights ($\overline{M}_n$s) and polydispersities were measured using a gel-permeation chromatography (GPC) system (Polymer Labs Model PL-GPC 210) calibrated by polystyrene standards. In the GPC measurements, tetrahydrofuran was used as the eluent.

3. Results and discussion

3.1. XANES spectroscopy

XANES spectroscopic measurements were carried out on the zinc glutarate catalysts synthesized in the present study. In addition, some zinc compounds (i.e., ZnO, anhydrous zinc acetate [$Zn(OAc)_2$], and zinc acetate dihydrate [$Zn(OAc)_2 \cdot 2H_2O$]) were chosen as references, and their XANES spectra were measured. The XANES spectra we obtained are displayed in Fig. 1.

In general, the XANES spectrum, which is the modulation of the photoabsorption coefficient between 0 and 50 eV above the absorption edge, is known to be produced by the excitation of core-level electrons into empty valence levels, quasi-bound states, and also by many-body excitation processes [43]. Further, the energy threshold E_0 is known to be affected by the charge distribution within the cluster, by the covalency or ionicity of the bonds, as well as by central atom effects such as many-body excitations, core relaxations, etc. The K-edge spectra of 3d transition elements show a preedge absorption feature, usually explained by electric dipole transitions to p-like states admixed to 3d states and by electric quadrupole coupling [44]. In contrast, the zinc atoms in zinc compounds do not produce any preedge structure. The completely filled 3d shells of the zinc atom prevent Zn $1s \rightarrow 3d$ transitions. Instead, the Zn $1s \rightarrow 4p$ transition produces an intense absorption structure, the so-called *white line* [45]. The white line intensity varies with transition probability, which is related to the complex geometry.

Fig. 1a shows the Zn K-edge spectra of the zinc reference samples. In these XANES spectra the white line (i.e.,

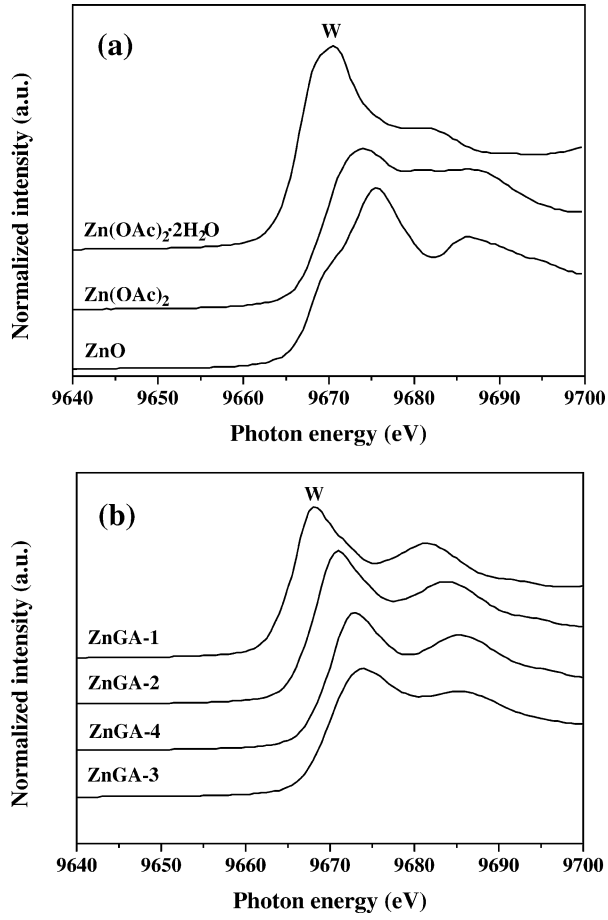

Fig. 1. X-ray absorption near-edge spectra of (a) some reference samples and (b) zinc glutarate catalysts at the Zn K-edge (W, white line).

the peak maximum marked by W in the figure) appears at 9670.6 eV for $Zn(OAc)_2 \cdot 2H_2O$, at 9673.9 eV for $Zn(OAc)_2$, and at 9675.5 eV for ZnO. As noted above, the energy shifts recorded in XANES spectra are generally affected by the oxidation state, bond character, and geometrical structure of the first shell around the central metal atom. $Zn(OAc)_2$ and ZnO are known to coordinate tetrahedrally rather than octahedrally. Compared to these two reference samples, the lower white line energy of $Zn(OAc)_2$ can be explained by the different effective nuclear charge produced by the larger extent of metal-to-ligand charge transfer in this species. Also, the white line of $Zn(OAc)_2 \cdot 2H_2O$, which has been reported to have a six-coordinate structure with a coordination geometry around the Zn atom that is approximately octahedral [46], occurs in a lower energy region than found for the other zinc reference samples. Thus, the white line energies of the reference samples are very sensitive to the local environment around each central Zn atom and are affected by the characteristics of the ligands.

As in Fig. 1a, all reference samples exhibit pronounced splitting of the white line, which is due to the orbital mixing of the central zinc atom. The octahedral $Zn(OAc)_2 \cdot 2H_2O$ sample produces a stronger white line intensity than the tetrahedrally coordinated $Zn(OAc)_2$ and ZnO samples. The white line intensity is known to vary with the space filling within the first coordination sphere [43]. Taking these facts into account, the differences between the white line intensities of the reference samples are attributed to differences in the first coordination spheres of their zinc atoms, namely to the structural difference between octahedral and tetrahedral coordination.

Fig. 1b displays the Zn K-edge spectra of the synthesized ZnGA catalysts. In these XANES spectra the white line (9668.0 eV) of ZnGA-1 occurs in a lower energy region than for the other ZnGA catalysts (ZnGA-2: 9670.9 eV; ZnGA-3: 9673.8 eV; ZnGA-4: 9672.7 eV). In addition, the intensity of the second peak relative to the white line intensity varies across the different catalysts as shown in Fig. 1b. Overall, the different catalysts show different XANES features in regard to the peak positions and intensities. It was concluded from the EXAFS results that all the catalysts except ZnGA-5 have coordination numbers close to 4 (within the error limit) (see Table 2); the energy variations of their white lines reflect the different oxidation states of the central Zn atoms. The Zn atoms in ZnGA-1 exhibited the most reduced state of the catalysts; these results might be related to the crystal perfection, as discussed later when we correlate these results with the XRD results.

Furthermore, all the catalysts exhibit clear splitting of the XANES spectrum white line, as was also observed for all the zinc reference samples. Such white line splitting has also been reported for other zinc complexes such as $(ImH)_4Zn^{2+}$ (ImH, imidazole), which has tetrahedral coordination [47]. The white line splitting exhibited by the Zn atoms of $(ImH)_4Zn^{2+}$ was attributed to $4p$–$4d$ mixing and/or to the involvement of the $5p$ level [47]. In line with this attribution, the white line splittings of the ZnGA catalysts might originate in part from $4p$–$4d$ mixing and/or from the involvement of the $5p$ level in the Zn atoms of the catalysts. For the square-planar symmetry of $3d$ transition metals [44,48], three distinct bands are usually observed, which correspond to the $1s \rightarrow 4p_z+$ "shake down" transition of metal-to-ligand charge transfer, the pure $1s \rightarrow 4p_z$ transition, and the $1s \rightarrow 4p_{x,y}$ transition. Therefore, the ZnGA catalysts in the present study do not appear to have square-planar geometries. Comparison of the XANES spectra of the ZnGA catalysts with those of the reference samples suggests that the local electronic structure of the Zn atoms in the catalysts resemble that found for $Zn(OR)_4$, which has tetrahedral coordination.

Collectively, the XANES spectral results lead to the conclusion that even though all ZnGA catalysts except ZnGA-4 have basically the same coordination geometry, the extent of coordination between the ligands and the Zn atoms is different for different synthetic routes. Details of the first-shell structures of the catalysts are discussed along with the EXAFS spectral results in the next section.

Table 2
Results of the curve fittings of EXAFS spectra obtained at room temperature

Sample	Pair	CN[a]	R (Å)[b]	σ^2 (pm^2)[c]
ZnGA-1	Zn–O	4.3	1.96	50
	Zn–C	6[d]	3.01	114
	Zn–C–O	–[e]	2.78	–[e]
	Zn–Zn	1	3.19	78
	Zn–O–Zn	–[e]	3.23	–[e]
ZnGA-2	Zn–O	4.2	1.95	40
	Zn–C	4[d]	3.00	72
	Zn–C–O	–[e]	3.16	–[e]
	Zn–Zn	1[d]	3.16	72
	Zn–O–Zn	–[e]	3.21	–[e]
ZnGA-3	Zn–O	4.0	1.96	54
	Zn–C	4[d]	3.09	19
	Zn–C–O	–[e]	2.92	–[e]
	Zn–Zn	1[d]	3.23	52
	Zn–O–Zn	–[e]	3.29	–[e]
ZnGA-4	Zn–O	4.8	1.96	65
	Zn–C	6[d]	2.87	105
	Zn–C–O	–[e]	2.64	–[e]
	Zn–Zn	1[d]	3.09	116
	Zn–O–Zn	–[e]	3.20	–[e]

[a] Coordination number (±0.5).
[b] Bond distance (±0.01 Å).
[c] The Debye–Waller factor.
[d] Obtained by the integer fitting method.
[e] The bond distance was acceptable.

3.2. Extended X-ray absorption fine structure spectroscopy

The analyses of the EXAFS spectra were performed using the FEFFIT program [49]. The k_3-multiplied, background-subtracted EXAFS spectra and their fitted profiles are displayed together in Fig. 2. The results of the curve fittings are summarized in Table 2.

In general, the single scattering process dominates for photon energies greater than 50 eV above the absorption edge. This is evident in the EXAFS spectra of the ZnGA catalysts shown in Fig. 2. Further, EXAFS spectra are usually influenced significantly by the coordination number of the metal atom and additionally by the relative intensity of the amplitude at the beginning of the EXAFS spectral region. Overall, the EXAFS modulation is essentially constant for all the catalysts, as shown in Fig. 2. Taking these considerations into account, the curve fittings of the EXAFS spectra show that the coordination number of oxygens around Zn atoms in all the catalysts is 4, except in the ZnGA-4 catalyst for which it is 5. The Debye–Waller factors and the bond distances were almost the same for all the catalysts within the error limit. This result suggests that the Zn atoms in the catalysts are tetrahedrally coordinated with oxygen despite their zinc and glutarate sources in the synthesis.

The curve fitting of multishells in r-space has been carried out according to the integer fitting method, in which the integer coordination number is floated to find the error minimum. Through the curve fittings it was found that the single scattering Zn–Zn and Zn–C contributions are significant. The combination of these results with the XANES results discussed in the earlier section suggests that the ZnGA catalysts have a network structure composed of layers interconnected by glutarate ligands having two carboxylate end groups. The first peak in the Fourier transforms contains information on the nearest neighboring oxygen of the zinc atoms. The zinc to oxygen distance for the catalysts is 1.96 Å. This value is typical of tetrahedrally coordinated Zn complexes (e.g., ZnO), and is shorter than that of purely ionic octahedral $Zn^{2+}O$ (ca. 2.12 Å) [50]. This distance and the Debye–Waller factor do not vary significantly with synthetic route. However, the coordination number of Zn–C is 4 for ZnGA-2 and ZnGA-3, which suggests tetrahedral coordination of the ligands. On the other hand, the coordination number of Zn–C is 6 for ZnGA-1 and ZnGA-4, which seems to be inconsistent with the results of the curve fit-

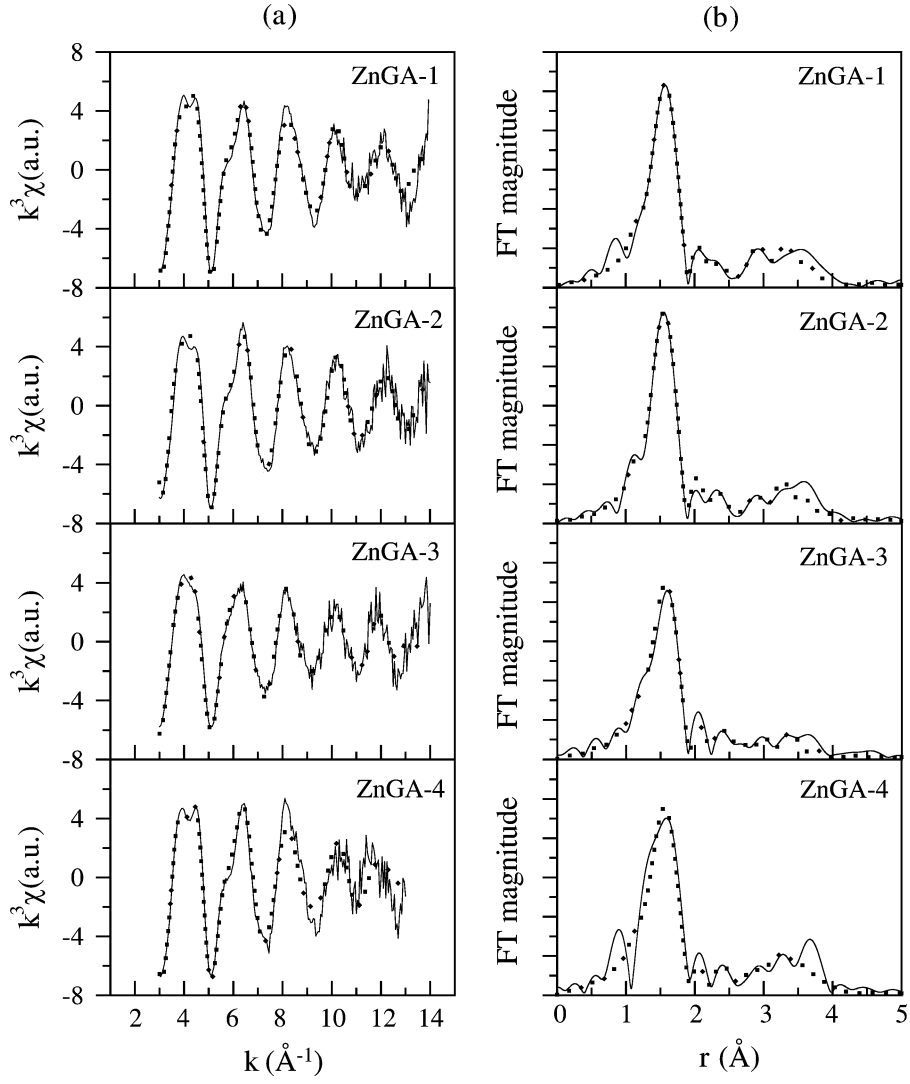

Fig. 2. (a) k^3-weighted EXAFS spectra (solid lines) and (b) their Fourier transforms (solid lines) of zinc glutarate catalysts ZnGA-1, Zn-GA-2, ZnGA-3, and ZnGA-4. The dotted lines denote the best fit model functions.

ting of the first shell in the EXAFS spectra. However, the high Zn–C coordination number also possibly indicates the presence nearby of carbon atoms from the alkylene group of the glutarate ligands coordinated with other Zn atoms, even though there may not be a direct Zn–C chemical bond. In addition, the contributions of Zn–O–Zn and Zn–C–O are detected even though their contributions are almost negligible. Collectively, the results again suggest that ZnGA catalysts are composed of a network structure. Further, the distance of these multiple scatterings reveals a large difference, depending on the type of ligands and the zinc sources.

3.3. Solid-state ^{13}C NMR spectroscopy

3.3.1. Zinc acetate and zinc monomethylglutarate (ZnGA-4)

To obtain local structural information for the Zn atoms in the ZnGA catalysts, anhydrous zinc acetate [$Zn(OAc)_2$] and zinc monomethylglutarate (i.e., ZnGA-4) were used as reference samples.

For anhydrous zinc acetate the ^{13}C CP-MAS spectrum shows a 1:1 splitting of the signals for both carboxyl (at 184.3 and 183.4 ppm) and methyl (at 23.4 and 21.7 ppm) carbons (data not shown), as previously reported by Hunt et al. [51]. This is consistent with the reported crystal structure with two crystallographically inequivalent methyl and carboxylate groups in the unit cell [51]. The carboxyl peak splitting for zinc acetate was attributed mainly to Zn–O distance differences rather than to conformational differences in the acetate ligand (e.g., OCO angles and CO distances) [51].

As shown in Fig. 3, the ^{13}C CP-MAS spectrum of zinc monomethylglutarate (ZnGA-4) also exhibits a 1:1 splitting of all carbon peaks except the one near 175 ppm; the peaks at 36.3 and 23.3 ppm, which are marked by asterisks, are from impurities which were absent in the spectrum of the fresh sample. Peaks are assigned as indicated in Fig. 3 and the FWHH data are summarized in Table 3. The carboxyl carbon peaks have less splitting (0–0.2 ppm) than that of the methyl carbon peak (0.4 ppm), as also observed in zinc acetate. These splittings are, however, smaller than those of

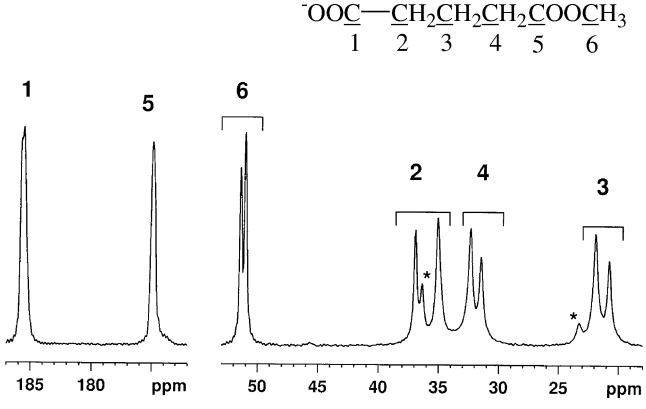

Fig. 3. ^{13}C CP-MAS spectrum of zinc mono-methyl glutarate with peak assignments. Peaks marked by an asterisk (∗) are due to impurities.

Table 3
Linewidth data of zinc glutarate catalysts measured by solid-state NMR spectroscopy

Compound	Peak position (ppm)	$FWHH_{obj}$[a] (Hz)	$FWHH_{inh}$[b] (Hz)
ZnGA-1	186.1	25	18
	185.3	26	18
	36.4	32	∼0
	34.4	12	–
	32.4	44	∼0
	23.4	36	∼0
	22.8	16	–
	20.3	57	∼0
ZnGA-2	186.1	47	39
	185.5	86	–
	38.6	33	–
	36.4	48	10
	34.6	28	–
	32.5	91	40
	23.4	73	19
	20.4	60	∼0
	19.8	16	–
ZnGA-3	186.1	50	43
	185.4	90	–
	183.7	23	–
	38.2	17	–
	36.4	62	20
	34.8	22	–
	32.6	95	41
	23.4	11	48
	20.3	13	43
ZnGA-4	185.8	17	12
	185.5	29	–
	174.9	31	27
	51.4	15	8
	51.0	17	7
	36.9	24	–
	36.3	31	–
	35.0	44	4
	32.4	47	∼0
	31.5	35	∼0
	23.3	56	∼0
	21.9	46	–
	20.8	41	∼0

[a] $FWHH_{obj}$ is the full width at half height (FWHH) of deconvoluted peaks in spectrum fitting with a Lorentzian line shape. The line broadening applied during the FT process was subtracted.

[b] $FWHH_{inh}$ was obtained by subtracting T_2 line broadening from the $FWHH_{obj}$.

zinc acetate. Furthermore, the further the methylene carbons are from the chelating carboxyl carbon, the less splitting is observed (1.9, 1.1, and 0.9 ppm). At least two inequivalent monomethylglutarate molecules should be in the unit cell; it is possible for inequivalent molecules to have a peak splitting too small to be resolved in a ^{13}C NMR spectrum. Possible causes of the crystallographic splitting are structural differences in ligand molecule conformation, in the ligand-binding configuration to the metal ions, and intermolecular packing effects. In general, conformation has a greater influence on chemical shift than intermolecular packing [52]. Thus the conformations of the methylene groups

closer to the chelating carboxylate carbon in the inequivalent monomethylglutarate molecules are expected to be different than those farther from the carboxylate carbon. The configurations of carboxylate binding to zinc atoms do not seem to vary in ZnGA-4, judging from the very small splitting of 0.2 ppm compared with the values reported for zinc acetate by Hunt et al. [51].

3.3.2. ZnGA catalysts

All the catalysts (ZnGA-1, ZnGA-2, and ZnGA-3) have similar ^{13}C CP-MAS spectra, as shown in Fig. 4. The carboxyl and central methylene carbon peaks of the glutarate groups appear near 185 and 20 ppm, respectively. The peaks of the other two methylene carbons occur in the 30–40 ppm region. Peak assignments are shown in Fig. 4a.

As shown in the deconvoluted spectra of Fig. 4, the central methylene carbon of each catalyst shows two well-defined singularities and an additional peak. This peak splitting suggests that the central methylene carbons in each catalyst are present at two or more crystallographically inequivalent sites in the unit cell.

The other carbons of the glutarate ligand also have peaks that are split into two or more component peaks. This peak splitting may arise because the carboxyl carbons at the two

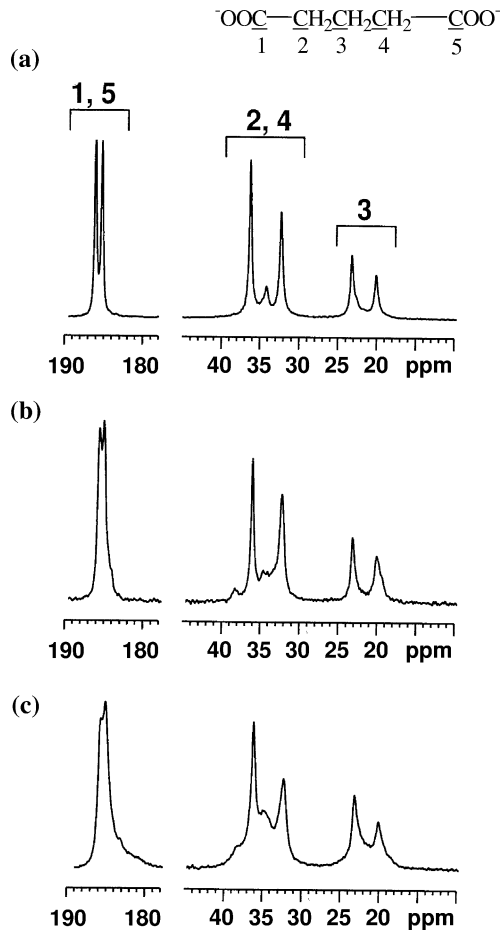

Fig. 4. ^{13}C CP-MAS spectra of zinc glutarate catalysts: (a) ZnGA-1; (b) ZnGA-2; (c) ZnGA-3.

ends of the glutarate ligand have different chemical shifts due to their crystallographically different locations in the crystal. Another possibility is that the carboxyl carbons at the two ends happen to share crystallographically distinct sites. However, this possibility is unlikely, since it is difficult to have the same crystallographic sites for carboxyl carbons at both ends when all methylene carbons in the glutarate ligand show crystallographic splitting.

On the other hand, note that the peak for the carboxyl carbons of the glutarate ligands exhibits little crystallographic peak splitting, compared to the peaks of the ligand's methylene carbons (see Fig. 4). The minimal crystallographic splitting for the carboxyl carbon is not surprising since even the model compounds we studied here (zinc acetate and zinc monomethylglutarate) have carboxyl carbon peaks with much smaller crystallographic splitting than the peaks for their methyl or methylene carbons. However, as shown in Figs. 3 and 4, the splitting of the carboxyl carbon peaks is still greater than that of the peak for the carboxyl carbons bound to zinc atoms in zinc monomethylglutarate (i.e., ZnGA-4). Such greater peak splitting might be due to a greater conformational difference between the carboxyl carbons at crystallographically inequivalent sites in the unit cell. The peak splitting could also be partly due to the diversity of metal-ligand binding modes, i.e., *syn–syn* and *syn–anti* bridging bidentate bonds, in the catalysts. According to a previous report [33], the ZnGA catalysts consist of both *syn–syn* and *syn–anti* bridging bidentate bonds but the population of *syn–syn* bridges is greater than that of *syn–anti* bridges. Zinc monomethylglutarate is also known to consist of both *syn–syn* and *syn–anti* bridging bidentate bonds [33]. However, zinc monomethylglutarate has a smaller population of bridge bonds than the ZnGA catalysts because the monomethylglutarate ligand has only a single carboxylate group that can bind with zinc atoms in comparison with the glutarate ligand which has two carboxylate groups and, furthermore, may have a different population ratio of *syn–syn* to *syn–anti* bridges from the ZnGA catalysts. In addition, the two chelating carboxyl groups of the glutarate ligands in the catalysts can be bonded to the same or different zinc metal ions. This could also contribute in part to the peak splitting for the carboxyl carbons.

These results indicate that both overall crystallinity and crystal quality (namely, size and perfection of crystals) are dependent upon synthetic route.

The $FWHH_{inh}$ results are summarized in Table 3. These linewidths were obtained by subtracting the line broadening applied during the FT process and natural linewidths appearing as a T_2 process from linewidths in lineshape fitting. As shown in Table 3, the ZnGA-1 catalyst has the smallest value of $FWHH_{inh}$ while ZnGA-3 shows the largest value of $FWHH_{inh}$. ZnGA-2 exhibits an intermediate value of $FWHH_{inh}$. The linewidth is directly related to structural inhomogeneity: in general, larger structural inhomogeneity causes wider linewidth. In the case of ZnGA catalysts composed of crystals, the linewidth is affected by the overall

Table 4
Relaxation data of zinc glutarate catalysts, as measured by solid-state NMR spectroscopy

Compound	Peak position (ppm)	T_2 (ms)	T_1 (s)	$T_{1\rho}(^1H)$ (ms)	$T_{1\rho}(^{13}C)$ (ms)
ZnGA-1	186.1	48	4×10^3	2.7×10^2	2.7×10^2
	185.3	38		2.8×10^2	3.3×10^2
	36.4	8.4	3×10^3	5.3×10^2	30
	34.4	5.5		2.2×10^2	25
	32.4	6.7		5.3×10^2	32
	23.4	5.7	3×10^3	4.3×10^2	27
	22.8				
	20.3	4.2		3.8×10^2	22
ZnGA-2	186.1	41	3×10^3	1.5×10^2	2.3×10^2
	185.5				
	38.6				
	36.4	8.4	2×10^3	2.6×10^2	26
	34.6				
	32.5	6.2		2.4×10^2	
	23.4	5.9	2×10^3	3.1×10^2	23
	20.4	4.4		2.0×10^2	19
	19.8				
ZnGA-3	186.1	48	6×10^2	56	3.0×10^2
	185.4				
	183.7				
	38.2				
	36.4	7.5	8×10^2	56	27
	34.8				
	32.6	5.9		85	27
	23.4	5.1	7×10^2	53	26
	20.3	3.7		73	22
ZnGA-4	185.8	66	3×10^3	3.5×10^2	2.8×10^2
	185.5				
	174.9	86		4.8×10^2	2.4×10^2
	51.4	43		4.8×10^2	1.7×10^2
	51.0	31		6.1×10^2	2.1×10^2
	36.9	9.6	2×10^3	4.1×10^2	26
	36.3				
	35.0	7.9		6.1×10^2	24
	32.4	6.8		3.7×10^2	21
	31.5	5.5		3.2×10^2	19
	23.3				
	21.9	5.5	2×10^3	3.2×10^2	25
	20.8	5.2		2.3×10^2	18

crystallinity and crystal quality (i.e., size and perfection of crystals) of the catalyst; a smaller $FWHH_{inh}$ value originates in larger crystallinity and better crystal quality. Therefore, the $FWHH_{inh}$ results suggest that the crystallinity and crystal quality (i.e., structural homogeneity) of the catalysts are, in decreasing order, ZnGA-1 > ZnGA-2 > ZnGA-3. This trend in crystallinity and crystal quality coincides with those measured from X-ray diffraction [30].

Relaxation data are listed in Table 4. As seen in Table 4, $T_1(^{13}C)$ of ZnGA-1 is longest while that of ZnGA-3 is shortest. $T_{1\rho}(^1H)$ shows the same trend: ZnGA-1 has the longest $T_{1\rho}(^1H)$ and ZnGA-3 has the shortest. When the structure of a crystal is highly inhomogeneous, more molecular motions tend to occur and those motions tend to have shorter relaxation times [52]. Therefore, the relaxation times measured for the ZnGA catalysts might be mainly due to their crystallinity and crystal quality; the fact that ZnGA-1 exhibits the longest relaxation time is due to its higher crystallinity and crystal quality (i.e., greater structural homogeneity), while the shortest relaxation time, that of ZnGA-3, is due to its low crystallinity and crystal quality.

In contrast, ZnGA-2 has the shortest $T_{1\rho}(^{13}C)$. The $T_{1\rho}(^{13}C)$ value of ZnGA-1 is longer than that of ZnGA-3. This trend in the $T_{1\rho}(^{13}C)$ data deviates from the expectation based on the $T_1(^{13}C)$ and $T_{1\rho}(^1H)$ data described above, as well as on the crystallinities measured by X-ray diffraction. In general, $T_1(^{13}C)$ is sensitive to motions near the ^{13}C Larmor frequency ($\sim$ 100 MHz in our case) at the given magnetic field strength, while $T_{1\rho}$ is known to be sensitive to motions near the RF spin–lock frequency ($\sim$ 50 kHz in our case). Therefore, the deviation of the $T_{1\rho}(^{13}C)$ data from expectation can be explained if $T_{1\rho}(^{13}C)$ is mainly determined by $T_{1\rho}(^{13}C)_{spin-spin}$ when $T_{1\rho}(^{13}C)^{-1} = T_{1\rho}(^{13}C)^{-1}_{spin-lattice} + T_{1\rho}(^{13}C)^{-1}_{spin-spin}$. The spin–lattice term arises from the modulation of internuclear dipolar interactions by molecular motion near the RF spin–lock frequency while the spin–spin term arises from a depolarization process of carbons to protons. This explanation is consistent with the low T_{CH} values (23–30 μs) of methylene carbons measured at 7.05 T, where T_{CH} is the cross-polarization time [53].

3.4. Surface area

For the ZnGA catalysts, surface areas were measured by the BET technique. ZnGA-3 had the highest surface area, 34.09 m^2/g, whereas the others catalysts had surface areas in the range 19.38–19.78 m^2/g. The surface areas of the catalysts are, in decreasing order, ZnGA-3 (34.09 m^2/g) > ZnGA-1 (19.78 m^2/g) $\approx$ ZnGA-2 (19.38 m^2/g).

3.5. Catalytic activities in the copolymerization of CO_2 and PO

The catalytic activities of the zinc glutarate catalysts synthesized from various zinc sources and glutaric acid derivatives were examined in the copolymerization of CO_2 with PO in excess. All the copolymerizations were carried out under optimized reaction conditions, as described in Table 5: 60 °C for 40 h under a CO_2 pressure of 51.5 atm. Characterizations of the obtained polymer products are summarized in Table 5. For each copolymerization, a polymer product that was insoluble in methanol was obtained at > 99 wt% of the total reaction products. The methanol-insoluble polymer products were identified by using ^1H NMR and ^{13}C NMR spectroscopy as alternating poly(propylene carbonate)s (PPCs), containing no ether linkages on the polymer backbone: ^1H NMR (δ, $CDCl_3$), 1.56 (3H; C$\underline{H}_3$), 4.20 (2H; C$\underline{H}_2$CH), 5.00 (1H; $CH_2C\underline{H}$); ^{13}C NMR (δ, C_6D_6), 16.9 ($\underline{C}H_3$), 70.1 ($CH_2\underline{C}H$), 73.5 ($\underline{C}H_2CH$), 155.7 (O$\underline{C}$OO).

Table 5
Polymerization of carbon dioxide (CO_2) and propylene oxide (PO) using zinc glutarate catalysts prepared from various zinc compounds and glutaric acid derivatives

Cat. No.	Weight of cat. (g)	Volume of PO (mL)	Pressure of CO_2 (atm)	Solvent	Reaction temperature (°C)	Reaction time (h)	Yield (g/g of cat.)[a]	$\frac{\overline{M}_n}{\overline{M}_w}$/PDI[b]
ZnGA-1	1.00	100	51.5	None	60	40	64	143K/343K/2.4
ZnGA-2	1.00	100	51.5	None	60	40	15.4	45K/315K/7.0
ZnGA-3	1.00	100	51.5	None	60	40	2.5	11K/124K/11.3
ZnGA-4	1.00	100	51.5	None	60	40	9.7	23K/82K/3.5

[a] Yield of alternating poly(propylene carbonate) insoluble in methanol.
[b] Measured by GPC calibrated with polystyrene standards.

As shown in Table 5, the copolymerization of CO_2 and PO was found to depend strongly upon the synthetic history of the zinc glutarate catalyst used. Copolymerization with ZnGA-1 produced PPC with 143,000 $\overline{M}_n$ and 2.4 polydispersity (PDI, $\overline{M}_w/\overline{M}_n$) with a yield of 64 g per gram of catalyst. However, the other catalysts provided PPCs of relatively low molecular weight and large polydispersity with low yields of 2.5–15.4 g per gram of catalyst.

It is generally accepted that the catalytic activity of a heterogeneous catalyst is primarily determined by its surface area; a larger catalyst surface area results in higher catalytic activity. It is thus very surprising that ZnGA-1 is the most effective catalyst for the copolymerization, delivering high molecular weight PPC in an exceptionally high yield, despite its relatively low surface area. In contrast, the ZnGA-3 catalyst has the largest surface area but is very much less effective, producing low-molecular-weight PPC with a very low yield. Therefore, the catalytic activities of the zinc glutarates in the copolymerization seem to be primarily dependent on their morphological structures rather than on their surface areas. Taking this into account, the surface areas of zinc glutarates may play an important role in improving the catalytic activity in the copolymerization when they meet first to have high crystallinity and good crystal quality.

The use of ZnO and glutaric acid in the synthesis produced a ZnGA-1 catalyst, which has the highest crystallinity and the best crystal quality of the synthesized catalysts. Further, the local structure around Zn atoms in the ZnGA-1 catalyst is slightly different from the structures found in the zinc glutarate catalysts (ZnGA-2 and ZnGA-3) derived from the other zinc and glutarate sources, as discussed in the earlier sections. It turns out that the morphological structure (local structure of the Zn active site, crystallinity, crystal size and perfection, etc.) of zinc glutarate, which is the critical factor determining the catalytic activity, is significantly influenced by all the factors involved in the synthesis, such as zinc source, glutarate source, and reaction conditions.

In conclusion, the zinc glutarate that was synthesized from ZnO and GA is the most active catalyst for the copolymerization of CO_2 and PO. The catalytic activity of this zinc glutarate may be further improved when its surface area is increased by the size reduction with retaining its high crystallinity and crystal quality.

4. Conclusions

Zinc glutarates synthesized from various zinc sources were investigated by X-ray absorption spectroscopy and solid-state CP-MAS ^{13}C NMR spectroscopy in order to characterize their local and microstructures. The X-ray absorption spectroscopic results for the local electronic structure indicate that the Zn atoms in all the zinc glutarate catalysts are tetrahedrally coordinated with the carboxyl oxygens of the glutarate ligands, and the Zn–O distances for all the catalysts are in the range 1.95–1.96 Å. Furthermore, the nearest neighbor Zn ions are separated by 3.19–3.23 Å. These results for the local structure suggest that ZnGA catalysts have a network structure composed of layers interconnected by glutarate ligands with two carboxylate end groups.

However, the observations of the Zn K-edge and the Zn–C coordination number variations among the catalysts are clues for the presence of differing first-shell structures around the Zn metal ions. The presence of such local structural differences in the catalysts was also monitored by analyzing solid-state ^{13}C NMR spectra, which exhibit peak splittings for all the carbon atoms of the glutarate ligand coordinated to the Zn metal ion. These local structural differences might originate from the differing levels of crystallinity and crystal quality (crystal size and perfection), which depend on the synthetic history of the catalysts. The crystallinity and crystal quality were found by X-ray diffraction to decrease in the order ZnGA-1 > ZnGA-2 > ZnGA-3. The differences in crystallinity and crystal quality are reflected in the solid-state NMR spectra; larger crystallinity and better crystal quality produce longer $T_{1\rho}(^1H)$ and $T_1(^{13}C)$.

The surface areas of the catalysts also vary, depending on their synthetic route. The surface areas were, in decreasing order, ZnGA-3 > ZnGA-1 ≈ ZnGA-2.

In the copolymerization of CO_2 and PO, the ZnGA-1 catalyst, which has low surface area, showed the highest catalytic activity, while the ZnGA-3 catalyst, which has the largest surface area, showed the lowest catalytic activity. For a heterogeneous catalyst, larger surface area generally produces higher catalytic activity. Taking this fact into account, the observed catalytic activities of the ZnGA catalysts are exceptional.

Therefore, the catalytic activities of the zinc glutarates for this copolymerization seem to depend primarily on their morphological structure (local structure, crystallinity, crystal size and perfection, etc.) rather than on their surface area. The morphological structure is significantly affected by all the factors in the synthesis of these catalysts, such as the zinc source, the glutarate source, and the reaction conditions. When zinc glutarates meet first to have high crystallinity and good crystal quality, their surface areas may play an important role in improving the catalytic activity in the copolymerization.

Acknowledgments

This study was supported by the Center for Integrated Molecular Systems (KOSEF) and by the Ministry of Education (BK21 Program). The X-ray absorption spectroscopic measurements at Pohang Accelerator Laboratory were supported by POSCO and the Korean Ministry of Science & Technology. In addition, the authors thank Mr. Kee Sung Han at the KBSI for data reduction in the NMR spectroscopic analysis.

References

[1] J.T. Houghton, B.A. Callander, S.K. Varney (Eds.), Climate Change 1992: The Supplementary Report to the IPCC Scientific Assessment, Cambridge University Press, Cambridge, 1992.
[2] K. Kacholia, R.A. Reck, Climate Change 35 (1997) 53.
[3] W.S. Broecker, Science 278 (1997) 1582.
[4] B.D. Santer, et al., Nature 382 (1996) 39.
[5] G.A. Meehl, W.M. Washington, Nature 382 (1997) 56.
[6] M. Hanschild, H. Wenzel, Environmental Assessment of Products, Vol. 2, Chapman–Hall, London, 1997.
[7] C. Hanisch, Environmental Sci. Tech. 32 (1998) 20A, and references therein.
[8] J. Paul, C.M. Pradier (Eds.), Carbon Dioxide Chemistry: Environmental Issues, Royal Soc. Chemistry, Cambridge, UK, 1994.
[9] B. Hileman, Chem. Eng. News 75 (1997) 34.
[10] W. Keim, A. Behr, G. Schmitt, Grundlagen der Industriellen Chemie, Sale und Sauerlander, Aarau, Frankfurt, 1986.
[11] (a) S. Inoue, H. Koinuma, T. Tsuruta, J. Polym. Sci.: Polym. Lett. Ed. 7 (1969) 287;
(b) S. Inoue, H. Koinuma, T. Tsuruta, Makromol. Chem. 130 (1969) 210.
[12] M. Kobayashi, S. Inoue, T. Tsuruda, Macromolecules 4 (1971) 658.
[13] K. Soga, K. Hyakkoku, S. Ikeda, Macromol. Chem. 179 (1978) 2837.
[14] K. Soga, E. Imai, I. Hattori, Polym. J. 13 (1981) 407.
[15] A. Rokicki, W.J. Kuran, Macromol. Sci.-Rev. Macromol. Chem. C 21 (1981) 135.
[16] T. Aida, M. Ishikawa, S. Inoue, Macromolecules 19 (1986) 8.
[17] S.A. Motika, T.L. Pickering, A. Rokicki, B.K. Stein, US patent 5,026,676, 1991.
[18] A. Rokicki, US patent 4,943,677, 1990.
[19] H. Kawachi, S. Minami, J.N. Armor, A. Rokicki, B.K. Stein, US patent 4,981,948, 1991.
[20] X. Chen, Z. Shen, Y. Zhang, Macromolecules 24 (1991) 5305.
[21] Y.B. Lee, J.H. Choi, Kor. Ind. Eng. Chem. 7 (1996) 813.
[22] W. Kuran, in: J.C. Salamone (Ed.), Polymeric Materials Encyclopedia, CRC, New York, 1996, p. 6623.
[23] A.Y. Khodakov, J. Lynch, D. Bazin, B. Rebours, N. Zanier, B. Moisson, P. Chaumette, J. Catal. 168 (1997) 16.
[24] D.J. Darensbourg, N.W. Stafford, T. Katsurao, J. Mol. Catal. 104 (1995) L1.
[25] D.J. Darensbourg, M. Holtcamp, Macromolecules 28 (1995) 7577.
[26] D.J. Darensbourg, M.W. Holtcamp, Coord. Chem. Rev. 153 (1996) 155.
[27] M. Super, E. Berluche, C. Costello, E. Beckman, Macromolecules 30 (1997) 368.
[28] C.-S. Tan, T.-J. Hsu, Macromolecules 30 (1997) 3147.
[29] M. Cheng, E. Lobkovsky, G. Coates, J. Am. Chem. Soc. 120 (1998) 11018.
[30] M. Ree, J.Y. Bae, J.H. Jung, T.J. Shin, J. Polym. Sci. Part A 37 (1999) 1863.
[31] D.J. Darensbourg, M.W. Holtcamp, G.E. Struck, M.S. Zimmer, S.A. Niezgoda, P. Rainey, J.B. Robertson, J.D. Draper, J.H. Reibenspies, J. Am. Chem. Soc. 121 (1999) 107.
[32] M. Ree, J.Y. Bae, J.H. Jung, T.J. Shin, Kor. Polym. J. 7 (1999) 333.
[33] M. Ree, J.Y. Bae, J.H. Jung, T.J. Shin, Y.-t. Hwang, T. Chang, Polym. Eng. Sci. 40 (2000) 1542.
[34] D. Darensbourg, J. Wildeson, J. Yarbrough, J. Reibenspies, J. Am. Chem. Soc. 122 (2000) 12487.
[35] Y.Z. Meng, L.C. Du, S.C. Tiong, Q. Zhu, A.S. Hay, J. Polym. Sci. Part A 40 (2002) 3579.
[36] M.H. Chisholm, D. Navarro-Llobet, Z. Zhou, Macromolecules 35 (2002) 6494.
[37] J.M. Lee, N.-E. Sung, J.-K. Park, J.-G. Yoon, J.-H. Kim, M.-H. Choi, K.-B. Lee, J. Synchrotron Rad. 5 (1998) 524.
[38] A. Frenkel, E.A. Stern, A. Voronel, M. Qian, M. Newville, Phys. Rev. B 48 (1993) 12449.
[39] J.J. Rehr, R.C. Albers, S.I. Zabinsky, Phys. Rev. Lett. 69 (1992) 3397.
[40] B.K. Teo, EXAFS: Basic Principles and Data Analysis, Springer, Berlin, 1986.
[41] (a) E.O. Stejskal, J.D. Memory, in: High Resolution NMR in the Solid State: Fundamentals of CP/MAS, Oxford University, Oxford, 1994, p. 83;
(b) R.A. Komoroski, in: Methods in Stereochemical Analysis, Vol. 7: High Resolution NMR Spectroscopy of Synthetic Polymers in Bulk, VCH, Deerfield Beach, FL, 1986, p. 194.
[42] B.H. Davis, Chem. Tech. (Jan. 1991) 18.
[43] (a) C. Hennig, K.-H. Hallmeier, G. Zahn, F. Tschwatschal, H. Hennig, Inorg. Chem. 38 (1999) 38;
(b) C. Hennig, F. Thiel, K.H. Hallmeier, R. Szargan, A. Hagen, F. Roessner, Spectrochim. Acta A 49 (1993) 1495.
[44] S.E. Shadle, J.E. Penner-Hahn, H.J. Schugar, B. Hedman, K.O. Hodgson, E.I. Solomon, J. Am. Chem. Soc. 115 (1993) 767.
[45] A. Bianconi, XANES Spectroscopy, in: D.C. Koningsberger, R. Prins (Eds.), X-Ray Absorption, Wiley, New York, 1986.
[46] T. Ishioka, Y. Shibata, M. Tkahashi, I. Kanesaka, Y. Kitagawa, K. Nakamura, Spectrochim. Acta 54A (1998) 1827.
[47] F.A. Cotton, H.P. Hanson, J. Chem. Phys. 28 (1958) 83.
[48] C. Cartier, M. Momenteau, E. Dartyge, A. Fontaine, G. Trouillon, A. Michalowicz, M. Verdaguer, Biochim. Biophys. Acta 119 (1992) 169.
[49] M. Newville, B. Ravel, D. Haskel, J.J. Rehr, E.A. Stern, Y. Yacoby, Physica B 208–209 (1995) 154.
[50] P. Porta, S. Morpurgo, I. Pettiti, J. Solid State Chem. 121 (1996) 372.
[51] P.A. Hunt, B.P. Straughan, A.A.M. Ali, R.K. Harris, B.J. Say, J. Chem. Soc., Dalton Trans. (1990) 2131.
[52] Aln.E. Tonelli, NMR Spectroscopy and Polymer Microstructure: The Conformational Connection, VCH, New York, 1989, Vol. 24 (1991) 5305.
[53] (a) P. Diehl, E. Fluck, H. Gunther, R. Kosfeld, J. Seelig (Eds.), NMR Basic Principles and Progress, in: Solid State NMR I: Methods, Vol. 30, Springer, New York, 1994, pp. 65–73;
(b) F. Laupretre, L. Monnerie, J. Virlet, Macromolecules 17 (1984) 1397.